UDC 662.756.3:544.47
DOI: 10.15587/1729-4061.2026.364663

IDENTIFICATION OF RESPONSE SURFACE PATTERNS IN ULTRASOUND-ASSISTED TRANSESTERIFICATION OF CASTOR OIL USING CAO-MGO CATALYSTS DERIVED FROM BLOOD COCKLE SHELL AND LIMESTONE

Abdullah Faizal
Master of Engineering, PhD Candidate*
Department of Mechanical Engineering
Universitas Wahidiyah
KH Wachid Hasyim str., 121, Bandar Lor, Kec. Mojoroto, Kota Kediri, Jawa Timur, Indonesia 64114
ORCID: https://orcid.org/0009-0003-4112-4413
Slamet Wahyudi
Corresponding author
Doctor of Engineering, Professor*
E-mail: slamet_w72@ub.ac.id
ORCID: https://orcid.org/0000-0003-4479-0895
Winarto Winarto
Doctor of Philosophy (PhD), Engineer, Associate Professor*
ORCID: https://orcid.org/0000-0002-7988-1132
Ishardita Pambudi Tama
Doctor of Philosophy (PhD), Engineer, Associate Professor
Department of Industrial Engineering**
ORCID: https://orcid.org/0000-0002-8392-6890
*Department of Mechanical Engineering**
**Universitas Brawijaya
MT. Haryono str., 167, Malang, Indonesia, 65145

The object of this study is the ultrasound-assisted transesterification of castor oil (Ricinus communis) into biodiesel using heterogeneous catalysts derived from natural sources: blood cockle shells (Anadara granosa) from Pekanbaru and limestone from Bangkalan, Indonesia. The problem addressed is that directly calcined limestone produces low biodiesel yield without complex post-treatment, and whether ultrasonic irradiation can compensate for this has not been tested. Three catalysts (shell-derived CaO, limestone-derived CaO-MgO, and their 1:1 physical mixture) were calcined at 900°C, 5 h, characterized by X-ray diffraction, Scanning electron microscopy with energy-dispersive X-ray spectroscopy, and Fourier-transform infrared spectroscopy, and tested under ultrasonic irradiation at 28 kHz with 56.0 W effective power (calorimetric calibration, 100 W nominal). A central composite design (reaction time, catalyst loading) was employed for each catalyst. Mean yields were 95.4% (mixed), 93.2% (limestone), and 89.2% (shell). Response surface analysis revealed a maximum for limestone (97.9% at 93.9 min, 4.24 wt%), a saddle point for shell, and an inverted surface for the mixture. These distinct geometries arise from phase composition and active-site differences. Unlike prior work requiring calcination-hydration-dehydration and NiO impregnation, the limestone catalyst here achieved 93.2% yield by direct calcination and sonication alone, far exceeding the 16.45% reported without sonication. These findings apply to biodiesel production where shell and limestone are abundant, replacing complex catalyst post-treatment with direct calcination and sonication

Keywords: heterogeneous catalysis, sonication, blood cockle shell, calcined limestone, response surface methodology, calorimetric calibration

Received 25.03.2026
Received in revised form 02.06.2026
Accepted date 11.06.2026
Published date 29.06.2026

How to Cite: *Faizal, A., Wahyudi, S., Winarto, W., Tama, I. P. (2026). Identification of response surface patterns in ultrasound-assisted transesterification of castor oil using CaO-MgO catalysts derived from blood cockle shell and limestone. Eastern-European Journal of Enterprise Technologies, 3 (6 (141)), 23–33. https://doi.org/10.15587/1729-4061.2026.364663*

1. Introduction

Biodiesel produced by transesterification of vegetable oils with methanol can partially replace petroleum diesel and lower net carbon emissions [1]. As more countries tighten emission standards, demand for biodiesel feedstocks that do not compete with food crops has increased [2, 3]. Castor oil (Ricinus communis) fits this requirement: its high ricinoleic acid content (85–90%) gives it unusual methanol solubility, which helps drive transesterification at moderate temperatures [4, 5].

A practical obstacle is catalyst cost. Heterogeneous catalysts made from natural shells and limestone are far cheaper than reagent-grade oxides and can be recovered after the reaction [2, 3]. However, directly calcined limestone has shown poor activity without additional chemical treatment [4]. A separate obstacle concerns ultrasonic process intensification: acoustic cavitation can improve mixing between oil and methanol phases [6, 7], yet nearly all published studies report the nominal power printed on the equipment rather than the actual power reaching the liquid, so their results are hard to reproduce [5].

If both obstacles could be addressed, namely activating cheap natural catalysts through sonication while properly characterizing the acoustic power, castor oil biodiesel could be produced at lower cost with better reproducibility. Indonesia has abundant blood cockle shells in Riau and limestone deposits in Madura, making these precursors locally available and inexpensive [8].

Therefore, studies on the optimization of ultrasound-assisted castor oil transesterification using natural CaO-MgO catalysts under calibrated acoustic power are scientific relevant.

2. Literature review and problem statement

The paper [4] presents the results of research on castor oil composition. It is shown that ricinoleic acid at 80–90% gives it higher methanol miscibility than most vegetable oils. The

paper [9] shows that calcining shells above 900°C converts carbonate to calcium oxide, and this approach was used in [10], where mud clam shell CaO gave over 96% yield at 60°C in 2 h. A CaO-MgO system reached 98% conversion with better reusability than CaO alone [9]. Modified CaO from other natural sources has also achieved comparable activity for transesterification [11]. But there were unresolved issues related to whether such performance can be obtained from natural minerals without complex post-treatment. The reason this question remained open is that previous attempts with natural minerals have typically required multi-step post-treatment to reach high yields. For example, [11] used hydration of CaO to $Ca(OH)_2$ before transesterification, while [12] combined calcination-hydration-dehydration with PEG surfactant templating and NiO impregnation. The simpler direct-calcination route was thus left under-investigated.

The paper [12] presents the results of research on Madura limestone. It is shown that directly calcined limestone produced only 16.45% yield. The reason for this may be its small surface area (9 m^2/g), limiting accessible active sites. A second reason is that without such treatment, residual $CaCO_3$ and $Ca(OH)_2$ phases dilute the active CaO content, as evidenced by the low 16.45% yield in [12] before post-treatment. A way to overcome these difficulties can be calcination-hydration-dehydration with PEG surfactant and NiO impregnation, reaching 90% yield [12]. However, such multi-step post-treatments add cost and complexity.

A simpler way to overcome this limitation can be ultrasonic process intensification. The paper [7, 13] shows that acoustic cavitation disrupts the oil – methanol phase boundary. This approach was used in [13] for castor oil, and in [14] with MgO/CaO nanorods. Response surface methodology was applied in [15, 16] to optimize the process. A likely reason this combination has not been explored is that ultrasonic biodiesel studies typically report the acoustic power as nominal generator output without calorimetric calibration, which limits comparison across reactors and complicates the testing of low-activity catalysts, which response depends on the actual delivered energy. However, these studies either used reagent-grade catalysts or a single natural source, and none tested directly calcined limestone under sonication without additional chemical treatment.

What remains untested is whether sonication alone can compensate for the low surface area of directly calcined limestone. No study has tried a physical mixture of separately calcined shell CaO and limestone CaO-MgO, and blood cockle shell (*Anadara granosa*) has received little attention for castor oil transesterification. The likely reason these specific combinations have been overlooked is that prior work on shell-derived CaO focused on more readily available bivalves such as mud clam [10] and mussel, cockle, and scallop [17], while limestone studies typically used the mineral alone rather than blended with shell-derived CaO. As a result, the complementary phase compositions (pure CaO from shell versus CaO-MgO from limestone) have not been systematically compared in a single experimental framework.

All this suggests that it is advisable to conduct a study devoted to comparing shell-derived CaO, limestone-derived CaO-MgO, and their physical mixture for ultrasound-assisted castor oil transesterification under calibrated acoustic power, with response surface analysis to identify the optimization patterns governing each catalyst system.

3. The aim and objectives of the study

The aim of the study is to determine whether ultrasonic irradiation can compensate for the low activity of directly calcined natural limestone and to identify the response surface patterns for three catalyst systems from blood cockle shell and limestone. This will allow the development of a simpler and lower-cost route for biodiesel production using locally available natural precursors, replacing complex catalyst post-treatments with calorimetrically-calibrated ultrasonic processing.

To achieve this aim, the following objectives were accomplished:

– to prepare and characterize catalysts calcined at 900°C using XRD, SEM-EDX, and FTIR;

– to compare three catalyst systems under ultrasonic irradiation at 28 kHz;

– to investigate the effects of reaction time and catalyst loading using a central composite design with eigenvalue analysis.

4. Materials and methods

4. 1. The object and hypothesis of the study

The object of this study is the transesterification of castor oil into biodiesel under ultrasonic irradiation using heterogeneous catalysts from natural shell and limestone. The hypothesis is that ultrasonic irradiation at 28 kHz can compensate for the low surface area of directly calcined limestone, producing yields comparable to post-treated catalysts. Assumptions:

a) calorimetric calibration in water adequately represents acoustic power in the oil-methanol-catalyst system;

b) gravimetric yield approximates FAME conversion. Simplification: the reaction temperature was not controlled but allowed to rise from ambient to ~50°C by cavitation heating, accepted as representative of a practical batch process.

4. 2. Materials

Castor oil (*Ricinus communis*, cold-pressed, hexane-free) was purchased from PT Unggul Herbal Atsiri (Banyuwangi, East Java, Indonesia; acid value 0.8 mgKOH/g, saponification value 179.4 mgKOH/g, hydroxyl value 161.1 mgKOH/g, viscosity 0.678 Pa·s at 25°C). Methanol (AR grade, 99.98%, catalog A-1056) was purchased from PT Smart Lab Indonesia (Tangerang Selatan, Indonesia). Blood cockle shells (*Anadara granosa*) were collected from Pekanbaru, Riau. Limestone was obtained from Bangkalan, Madura.

4. 3. Methods

4. 3. 1. Catalyst preparation

Blood cockle shells were washed with distilled water and dried at 105°C overnight (~12 h). Limestone was cleaned and dried identically. Both were calcined separately at 900°C at 10°C/min for 5 h, ground and sieved to 100–200 mesh (74–149 μm), and stored in a desiccator. For the mixed catalyst, the powders were physically blended at 1:1 mass ratio.

4. 3. 2. Catalyst characterization

XRD was performed using a PANalytical X'Pert PRO with Cu-Kα (λ = 1.5406 Å) at 40 kV/35 mA, 2θ = 10–90° (codes XRD 1249 and 1250). SEM-EDX was conducted at 20 kV (codes MAP 442 and 443). FTIR was performed using a Shimadzu spectrometer at 4 cm^{-1} resolution with 40 scans over 400–4000 cm^{-1} with Happ-Genzel apodization (codes IR 918 and 919). All analyses were performed at the Laboratorium Mineral dan Material Maju, FMIPA, Universitas Negeri Malang.

4. 3. 3. Transesterification procedure

Castor oil (4.8 g) was mixed with methanol at a 15:1 molar ratio (2.47 g, based on the average molecular weight of castor oil of 938 g/mol calculated from the saponification value).

The reaction vessel was placed inside the ultrasonic bath filled with 3 L of water. The ultrasonic generator was set to its full output (nominal 100 W, effective 56.0 W at 28 kHz), and the reaction was allowed to proceed for the duration specified by the design. The reaction temperature was not externally controlled; it increased from ambient temperature (approximately 28°C) to approximately 50°C over the course of the reaction due to cavitation-induced heating.

The effective ultrasonic power dissipated into the reaction medium was determined by the calorimetric method. A known mass of water (3000 g) was placed in the ultrasonic bath, and the temperature rise was recorded at one-second intervals for approximately 15 minutes using a digital thermometer (precision ± 0.01°C). The effective power was calculated using (1)

$$P = m \times C_p \times \left(\frac{dT}{dt} \right), \quad (1)$$

where P – the dissipated acoustic power (W), m – the mass of water (g), C_p – the specific heat capacity of water (4.18 J·g^{-1}°C^{-1}), and dT/dt – the slope of the linear regression of the temperature–time data. Based on triplicate measurements, the effective acoustic power was determined to be 56.0 ± 4.2 W, corresponding to an energy transfer efficiency of approximately 56% from the nominal generator output.

At the end of the reaction, the mixture was transferred to a separation vessel and allowed to stand until phase separation occurred. The lower glycerol-rich layer was removed, while the upper crude biodiesel layer was collected. The crude biodiesel was washed three times using distilled water maintained at 50°C to remove residual methanol, catalyst particles, glycerol, soaps, and other water-soluble impurities. The washed biodiesel was subsequently heated at 105°C for 1 h to eliminate residual water and remaining volatile components. Finally, the dried biodiesel was weighed, and the yield was calculated as the ratio of dried biodiesel mass to the initial castor oil mass (2)

$$\text{Yield}(\%) = \left(\frac{\text{mass of dried biodiesel}}{\text{initial mass of castor oil}} \right) \times 100. \quad (2)$$

The yield values reported in this study represent the gravimetric yield based on dried product mass, rather than fatty acid methyl ester (FAME) purity determined by gas chromatography. Consequently, the reported values may slightly overestimate the true FAME yield due to the possible presence of trace residual methanol, moisture, soap, or other impurities not fully removed during washing and drying. All values in the experimental yield tables correspond to directly measured masses; no model-estimated or adjusted values were included.

The yields ranged from 80.8 to 99.8% (shell), 87.5 to 97.9% (limestone), and 89.4 to 99.8% (mixed). Notably, the limestone center-point replicates clustered at 97.5–97.9%, while the mixed catalyst center points gave only 89.4–89.8% with higher yields at the edges, suggesting distinct response surface geometries.

4. 3. 4. Experimental design

A CCD with two factors (time: 60–120 min; catalyst: 3–5 wt%) was employed: 17 runs per catalyst (8 factorial × 2 replications, 4 axial at α = 1.6818, 5 center points).

5. Results of catalyst characterization and response surface optimization

5. 1. Catalyst characterization

5. 1. 1. X-ray diffraction

Fig. 1 shows the XRD patterns. The limestone catalyst (XRD 1249) contains $CaCO_3$, CaO, $Ca(OH)_2$, and MgO. Peaks at 2θ ≈ 32.2°, 37.4°, 53.8°, 64.2°, 67.4° correspond to CaO [14]. A peak at 2θ ≈ 43° confirms MgO (periclase). This composition is matching the dolomitic character of Madura limestone described by [12]. The shell catalyst (XRD 1250) shows only $CaCO_3$ and CaO, without any Mg-bearing phases [17].

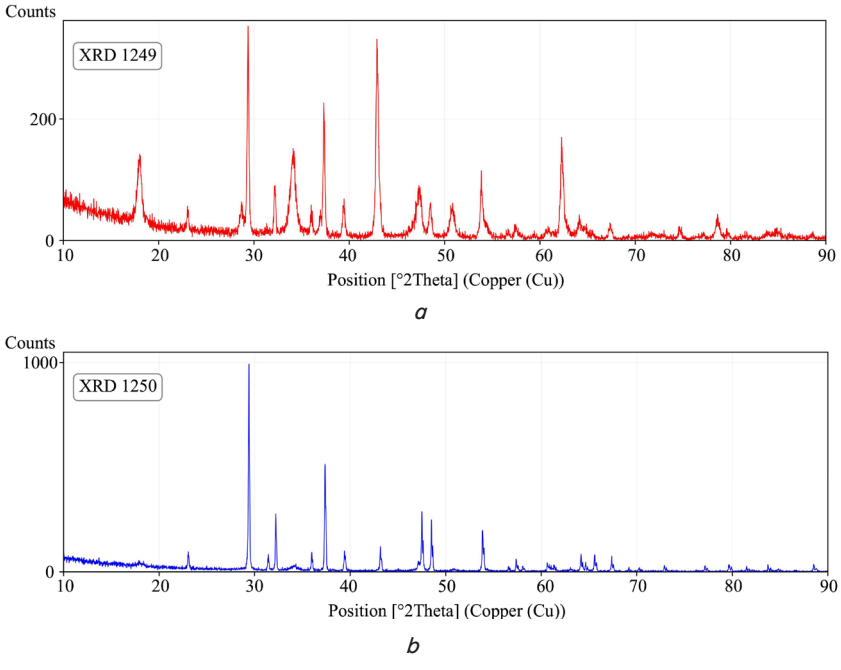

Fig. 1. X-ray diffraction patterns of the catalysts: *a* — limestone (XRD 1249); *b* — shell (XRD 1250)

The diffraction patterns confirm that the two precursors yield different phase compositions: limestone retains both CaO and MgO alongside residual $CaCO_3$ and $Ca(OH)_2$, whereas shell produces CaO with residual $CaCO_3$ only and no Mg-bearing phases, consistent with the purely aragonitic origin of *Anadara granosa*.

5. 1. 2. Scanning electron microscopy morphology

Fig. 2 shows the limestone catalyst at 50,000×: sub-micron granular aggregates (0.5–2 μm) typical of thermally decomposed dolomite. Fig. 3 shows the shell catalyst at 5,000×: larger plate-like lamellar fragments (10–50 μm) retaining biogenic growth structures, characteristic of calcined mollusk shells [14, 17].

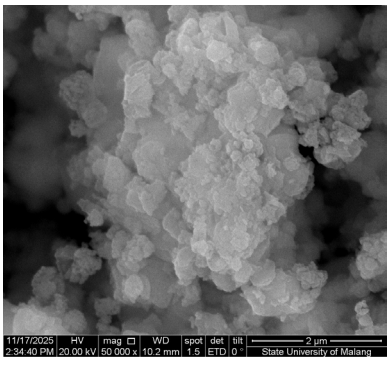

Fig. 2. Scanning electron microscopy micrograph of limestone catalyst (MAP 442, 50,000×, 2 μm)

The contrasting morphologies, sub-micron granular aggregates for limestone versus large plate-like fragments for shell, reflect their different precursor structures and suggest that the limestone catalyst has a higher specific surface area, which may contribute to its catalytic performance.

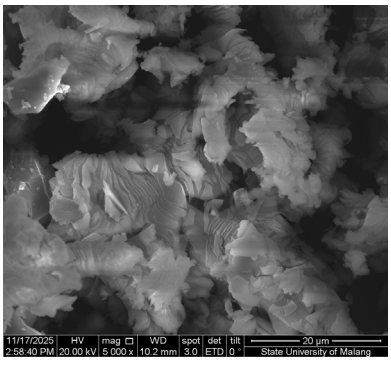

Fig. 3. Scanning electron microscopy micrograph of shell catalyst (MAP 443, 5,000×, 20 μm)

5. 1. 3. Energy-dispersive X-ray elemental analysis

EDX mapping (Fig. 4) detected four elements in the limestone catalyst: C (9.81 wt%), O (48.95 wt%), Mg (13.59 wt%), and Ca (27.65 wt%). The shell catalyst (Fig. 5) contained only C (12.31 wt%), O (44.27 wt%), and Ca (43.43 wt%) with no Mg detected, consistent with XRD results.

The elemental composition is presented in Table 1.

Table 1

EDX composition of limestone catalyst (MAP 442)

Element	Weight %	Atomic %
C K	9.81	15.93
O K	48.95	59.69
Mg K	13.59	10.91
Ca K	27.65	13.46

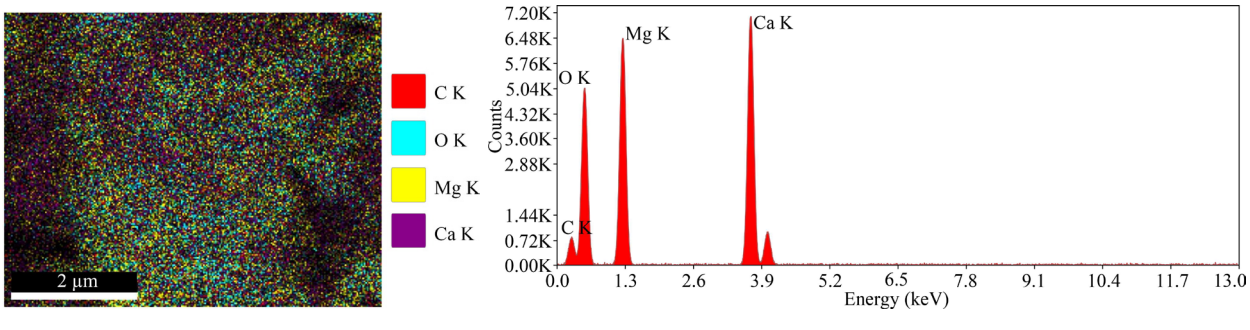

a *b*

Fig. 4. Energy-dispersive X-ray analysis of limestone catalyst (MAP 442): *a* — elemental mapping; *b* — sum spectrum

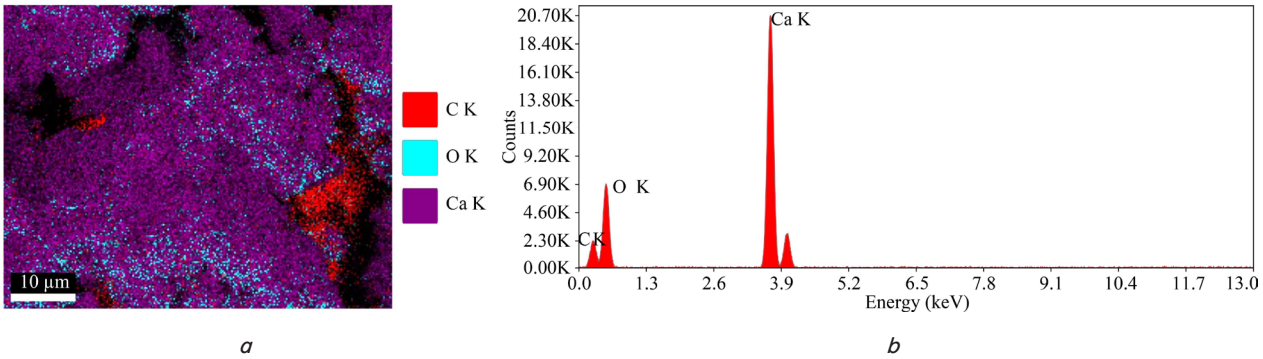

a *b*

Fig. 5. Energy-dispersive X-ray analysis of shell catalyst (MAP 443): *a* — elemental mapping; *b* — sum spectrum

The shell catalyst composition is given in Table 2.

Table 2

EDX composition of shell catalyst (MAP 443)

Element	Weight %	Atomic %
C K	12.31	21.02
O K	44.27	56.76
Ca K	43.43	22.23

The absence of magnesium in the shell catalyst confirms that CaO is the sole active phase, whereas the limestone catalyst contains both CaO and MgO. The higher calcium content in the shell (43.43 wt%) compared to limestone (27.65 wt%) reflects pure aragonite in shells versus dolomitic limestone containing both calcium and magnesium carbonates.

5. 1. 4. Fourier-transform infrared spectroscopy

Fig. 6, 7 present the FTIR spectra. Both spectra show strong bands at 1400 cm^{-1} (CO_3^{2-} asymmetric stretching ν_3), 875 cm^{-1} (CO_3^{2-} out-of-plane bending ν_2), 711 cm^{-1} (CO_3^{2-} in-plane bending ν_4), and 3643 cm^{-1} (O–H stretching of $Ca(OH)_2$), indicating residual $CaCO_3$ and $Ca(OH)_2$ in both catalysts [12]. The limestone spectrum also has a band at 470 cm^{-1} attributable to Ca-O/Mg-O lattice vibrations, which is absent in the shell catalyst, consistent with the presence of MgO detected by XRD and EDX.

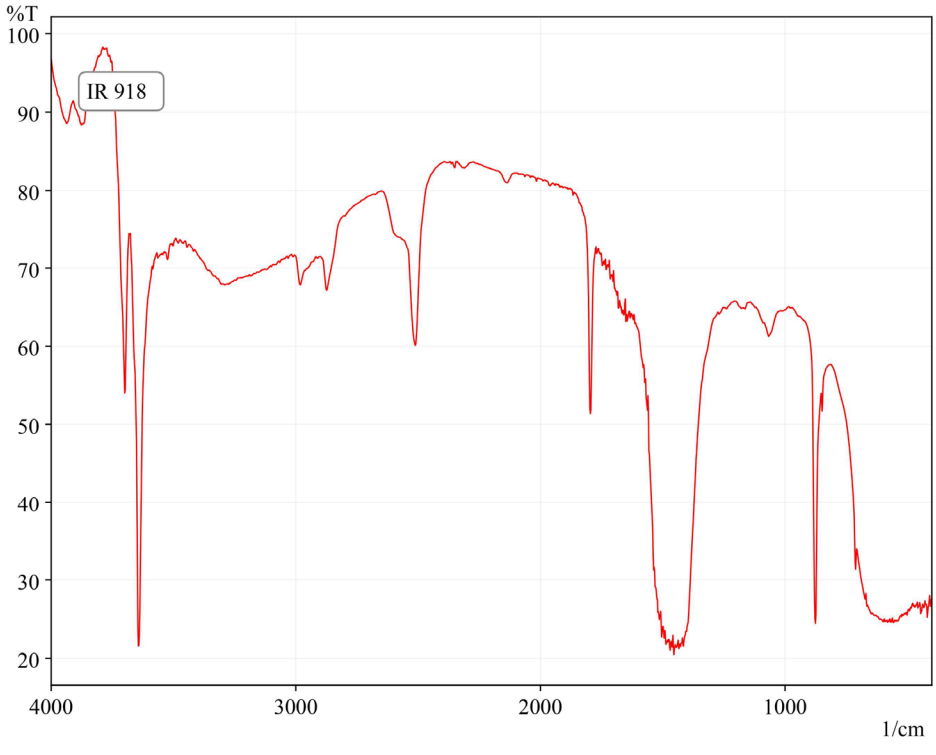

Fig. 6. Fourier-transform infrared spectrum of limestone catalyst (IR 918)

Table 3 summarizes the FTIR absorption bands identified in both catalysts and their corresponding functional group assignments based on published reference data for calcined calcium carbonate materials.

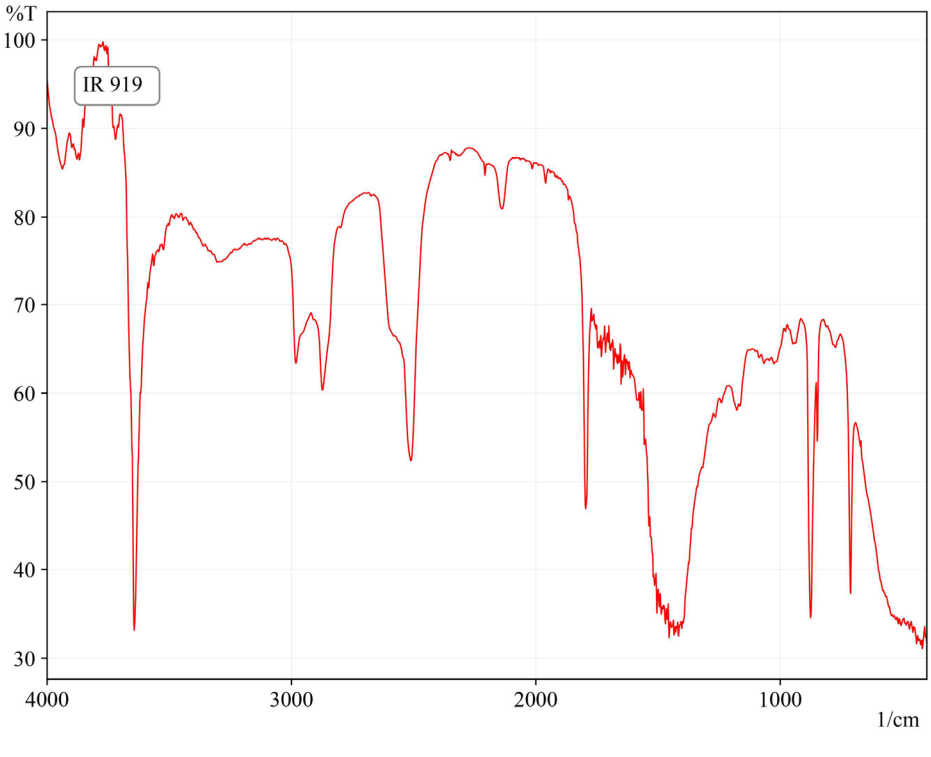

Fig. 7. Fourier-transform infrared spectrum of shell catalyst (IR 919)

Table 3

FTIR absorption bands and assignments for the limestone-derived and shell-derived catalysts

Wavenumber (cm^{-1})	IR 918 (Limestone)	IR 919 (Shell)	Intensity	Assignment
3643	✓	✓	Strong	O-H stretching, $Ca(OH)_2$
2982	✓	✓	Weak	C-H stretching
2874	✓	✓	Weak	C-H stretching
2511	✓	✓	Medium	CO_3^{2-} – combination band
1796	✓	✓	Medium	CO_3^{2-} combination band
1400	✓	✓	Very strong	CO_3^{2-} ν_3 asymmetric stretching
1067	✓	–	Medium	CO_3^{2-} symmetric stretching
876	✓	✓	Strong	CO_3^{2-} ν_2 out-of-plane bending
712	✓	✓	Medium	CO_3^{2-} ν_4 in-plane bending
471	✓	–	Medium	Ca-O/Mg-O lattice vibration

Note: ✓ – detected; "–" – not detected.

The key distinguishing feature between the two catalysts is the presence of absorption bands at 1067 and 471 cm^{-1} in the limestone spectrum that are absent in the shell spectrum. The band at 471 cm^{-1} is attributed to Ca-O/Mg-O lattice vibrations, providing additional spectroscopic evidence for the presence of MgO in the limestone-derived catalyst, consistent with XRD and EDX findings. The strong band at 3643 cm^{-1} in both spectra confirms the presence of $Ca(OH)_2$, indicating partial rehydration of CaO upon exposure to atmospheric moisture during handling and storage [12].

5. 2. Biodiesel yield

The experimental results presented in Tables 4–6 show the following yield ranges for the three catalyst systems.

Table 4

Shell-derived catalyst results

Run	Time (min)	Cat. (wt%)	US (W)	Oil (g)	MeOH (g)	Cat. (g)	BD (g)	Yield (%)
1	90	4	56.0	4.80	2.47	0.19	4.300	89.6
2	60	5	56.0	4.80	2.47	0.24	4.290	89.4
3	120	3	56.0	4.80	2.47	0.14	4.790	99.8
4	60	5	56.0	4.80	2.47	0.24	4.280	89.2
5	60	3	56.0	4.80	2.47	0.14	4.174	87.0
6	90	4	56.0	4.80	2.47	0.19	4.310	89.8
7	120	3	56.0	4.80	2.47	0.14	4.780	99.6
8	140.45	4	56.0	4.80	2.47	0.19	4.370	91.0
9	39.55	4	56.0	4.80	2.47	0.19	4.190	87.3
10	90	4	56.0	4.80	2.47	0.19	4.310	89.8
11	120	5	56.0	4.80	2.47	0.24	3.880	80.8
12	60	3	56.0	4.80	2.47	0.14	4.160	86.7
13	90	4	56.0	4.80	2.47	0.19	4.290	89.4
14	90	5.68	56.0	4.80	2.47	0.27	3.930	81.9
15	90	4	56.0	4.80	2.47	0.19	4.300	89.6
16	120	5	56.0	4.80	2.47	0.24	3.880	80.8
17	90	2.32	56.0	4.80	2.47	0.11	4.590	95.6

Table 5

Limestone-derived catalyst results

Run	Time (min)	Cat. (wt%)	US (W)	Oil (g)	MeOH (g)	Cat. (g)	BD (g)	Yield (%)
1	90	4	56.0	4.80	2.47	0.19	4.690	97.7
2	60	5	56.0	4.80	2.47	0.24	4.400	91.7
3	120	3	56.0	4.80	2.47	0.14	4.320	90.0
4	60	5	56.0	4.80	2.47	0.24	4.390	91.5
5	60	3	56.0	4.80	2.47	0.14	4.410	91.9
6	90	4	56.0	4.80	2.47	0.19	4.700	97.9
7	120	3	56.0	4.80	2.47	0.14	4.310	89.8
8	140.45	4	56.0	4.80	2.47	0.19	4.350	90.6
9	39.55	4	56.0	4.80	2.47	0.19	4.285	89.3
10	90	4	56.0	4.80	2.47	0.19	4.680	97.5
11	120	5	56.0	4.80	2.47	0.24	4.560	95.0
12	60	3	56.0	4.80	2.47	0.14	4.400	91.7
13	90	4	56.0	4.80	2.47	0.19	4.690	97.7
14	90	5.68	56.0	4.80	2.47	0.27	4.400	91.7
15	90	4	56.0	4.80	2.47	0.19	4.690	97.7
16	120	5	56.0	4.80	2.47	0.24	4.560	95.0
17	90	2.32	56.0	4.80	2.47	0.11	4.200	87.5

Table 6

Mixed catalyst (shell + limestone, 1:1) results

Run	Time (min)	Cat. (wt%)	US (W)	Oil (g)	MeOH (g)	Cat. (g)	BD (g)	Yield (%)
1	90	4	56.0	4.80	2.47	0.19	4.290	89.4
2	60	5	56.0	4.80	2.47	0.24	4.710	98.1
3	120	3	56.0	4.80	2.47	0.14	4.680	97.5
4	60	5	56.0	4.80	2.47	0.24	4.700	97.9
5	60	3	56.0	4.80	2.47	0.14	4.790	99.8
6	90	4	56.0	4.80	2.47	0.19	4.300	89.6
7	120	3	56.0	4.80	2.47	0.14	4.690	97.7
8	140.45	4	56.0	4.80	2.47	0.19	4.710	98.1
9	39.55	4	56.0	4.80	2.47	0.19	4.790	99.8
10	90	4	56.0	4.80	2.47	0.19	4.290	89.4
11	120	5	56.0	4.80	2.47	0.24	4.490	93.5
12	60	3	56.0	4.80	2.47	0.14	4.790	99.8
13	90	4	56.0	4.80	2.47	0.19	4.310	89.8
14	90	5.68	56.0	4.80	2.47	0.27	4.690	97.7
15	90	4	56.0	4.80	2.47	0.19	4.310	89.8
16	120	5	56.0	4.80	2.47	0.24	4.490	93.5
17	90	2.32	56.0	4.80	2.47	0.11	4.790	99.8

Note: Shell: 80.8–99.8% (mean 89.2 ± 5.4%). Limestone: 87.5–97.9% (mean 93.2 ± 3.5%). Mixed: 89.4–99.8% (mean 95.4 ± 4.3%). ANOVA: $F = 8.18$, $p < 0.05$. Mixed > shell ($t = 3.99$, $p < 0.05$); limestone > shell ($t = 2.56$, $p < 0.05$); limestone vs mixed: not significant ($t = 1.43$).

5. 3. Response surface analysis

Shell

$$Y = 89.62 + 1.11x_1 - 4.09x_2 - 0.16x_1^2 - -0.31x_2^2 - 5.33x_1x_2 \left(R^2 = 0.9996\right).$$

Limestone

$$Y = 97.70 + 0.40x_1 + 1.23x_2 - 2.75x_1^2 - -2.88x_2^2 + 1.33x_1x_2 \left(R^2 = 0.9992\right).$$

Mixed

$$Y = 89.82 - 1.18x_1 - 1.11x_2 + 3.49x_1^2 + +3.41x_2^2 - 0.57x_1x_2 \left(R^2 = 0.9598\right).$$

Limestone: maximum at 93.9 min, 4.24 wt% (97.9%). Shell: saddle point. Mixed: minimum at center, yields increasing toward edges.

The three-dimensional response surfaces (Fig. 8) and contour plots (Fig. 9) visually confirm these distinct geometries.

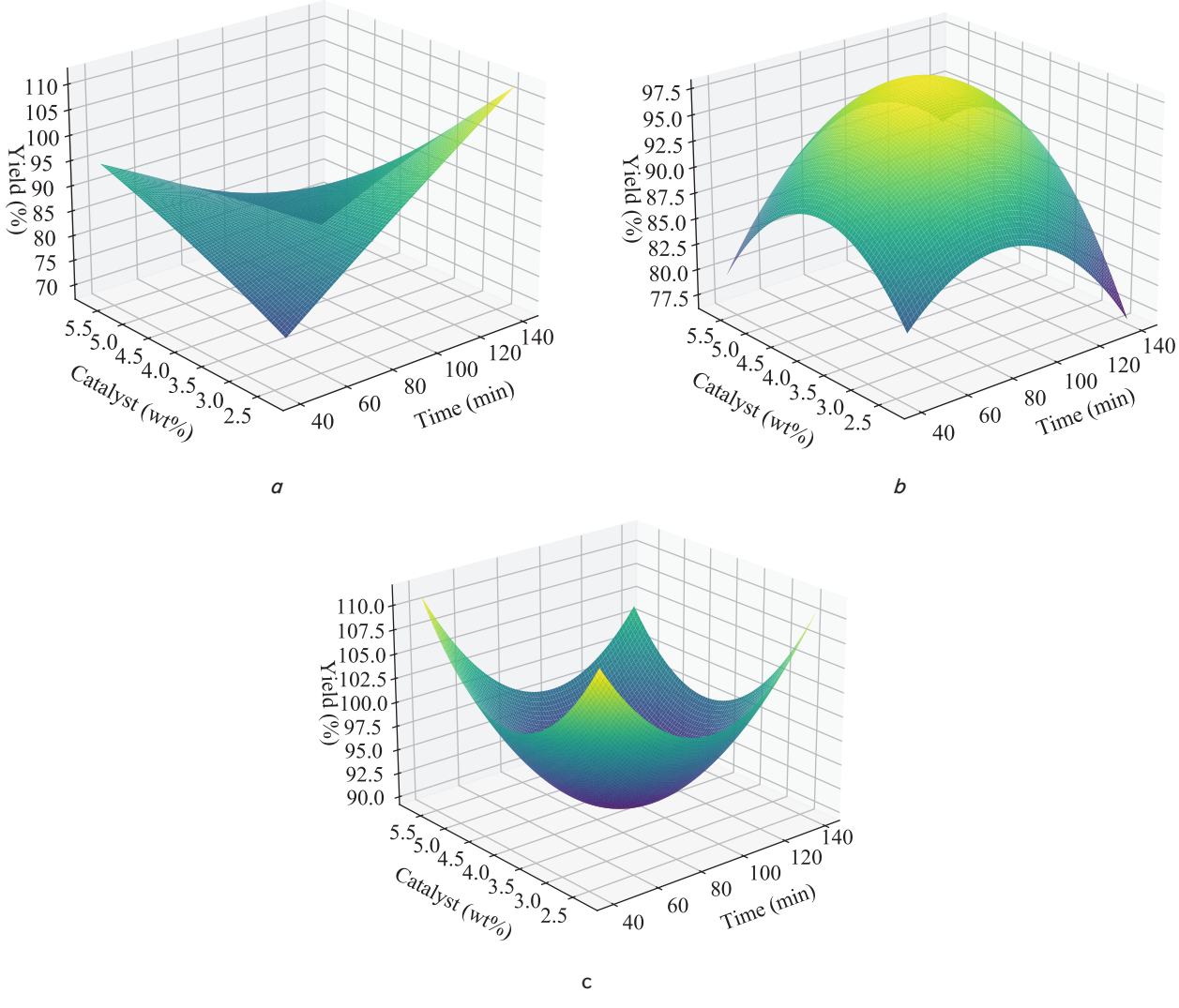

Fig. 8. Three-dimensional response surface plots: *a* — shell-derived catalyst; *b* — limestone-derived catalyst; *c* — mixed catalyst

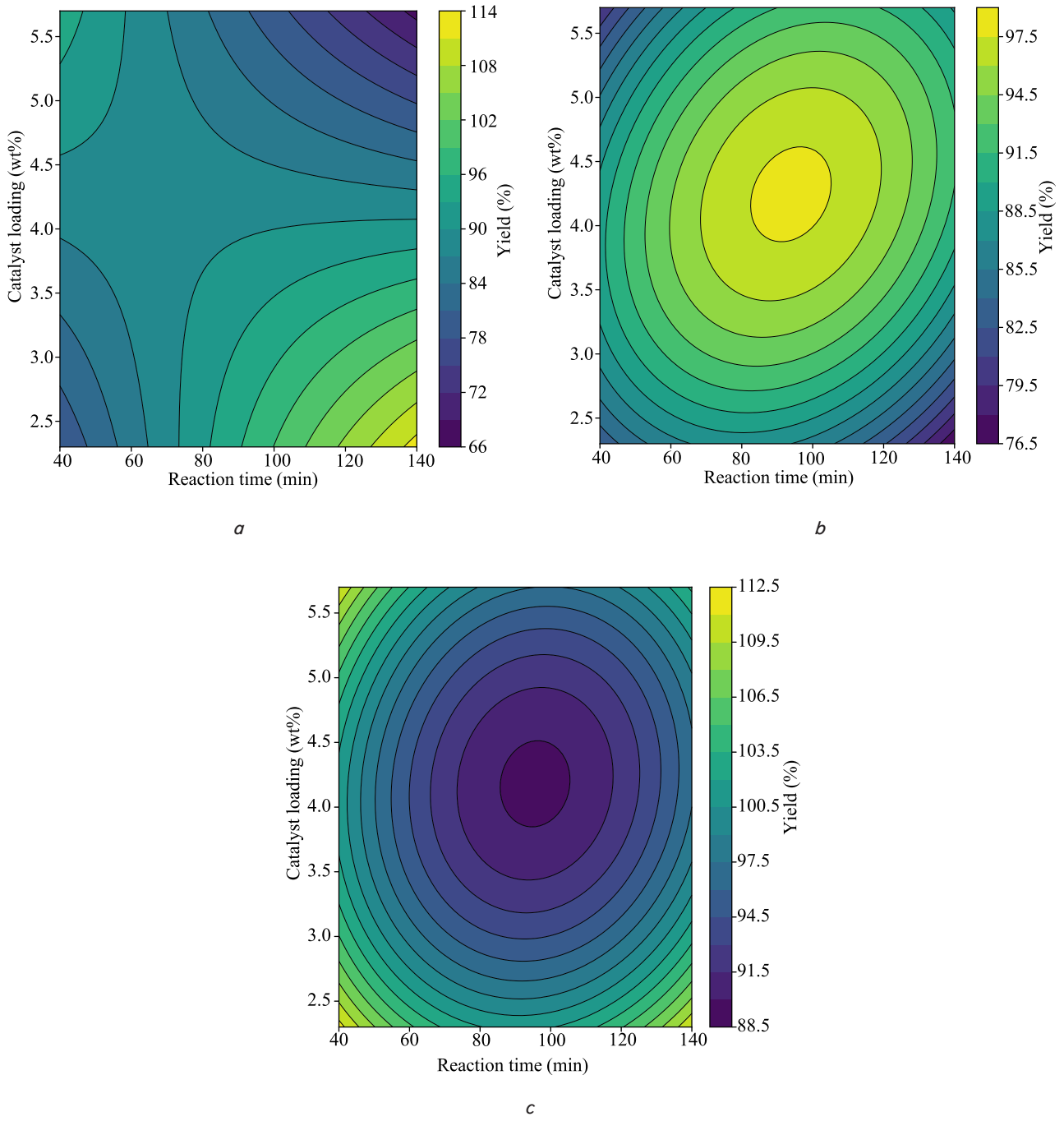

Fig. 9. Contour plots of biodiesel yield: *a* — shell-derived catalyst; *b* — limestone-derived catalyst; *c* — mixed catalyst

The contour plots confirm three distinct geometries: elliptical contours centered on a maximum for limestone, a saddle-shaped gradient for shell with yield rising toward low catalyst loading, and an inverted pattern for the mixed catalyst with a minimum at the center and yields increasing toward the design boundaries.

6. Discussion of catalyst performance and response surface geometry

The catalyst characterization results come from XRD patterns (Fig. 1), SEM micrographs (Fig. 2, 3), EDX spectra and quantification (Fig. 4, 5, Tables 1, 2), and FTIR spectra and band assignments (Fig. 6, 7, Table 3). All three methods agree that shell calcination at 900°C produces predominantly CaO (Ca 43.43 wt%, no Mg), while limestone yields mixed CaO-MgO (Ca 27.65 wt%, Mg 13.59 wt%). The FTIR band at 470 cm^{-1} in the limestone catalyst, absent in the shell, further corroborates the presence of MgO. These results are consistent with the dolomitic composition of Madura limestone reported in [12]. The SEM images show two very different particle shapes: sub-micron granular aggregates (limestone) versus plate-like lamellar fragments (shell).

The yield comparison gave mean values of 89.2, 93.2, and 95.4% for shell, limestone, and mixed catalysts, respectively (from individual-run data in Tables 4, 5, 6, computed via eq. (2)). These fall within the range reported elsewhere. In [10]

over 96% was achieved with clam shell CaO; in [9] up to 98% with CaO-MgO. Notably, the limestone catalyst in this study achieved a mean yield of 93.2% through direct calcination combined with ultrasonic irradiation, substantially exceeding the 16.45% reported in [12] for directly calcined Madura limestone without ultrasonic assistance. While in [12] CHD treatment with PEG surfactant and NiO impregnation were required to reach 90%, the present study shows that ultrasonic irradiation alone can compensate for the low surface area of directly calcined limestone by enhancing mass transfer through acoustic cavitation.

The effects of reaction time and catalyst loading were captured by the central composite design. The three catalysts gave different response surfaces, shown in Fig. 8 (3D) and Fig. 9 (contour projections). The limestone catalyst (Table 5, Fig. 8, *b*, 9, *b*) showed a convex surface with a clear maximum at 93.9 min and 4.24 wt% (predicted yield 97.9%). Both eigenvalues of the Hessian matrix were negative ($\lambda_1 = -4.29$, $\lambda_2 = -6.96$), confirming a genuine maximum. This means the center of the design space is near-optimal for limestone, and pushing further would bring only small gains.

The shell catalyst had a saddle point (Table 4; Fig. 8, *a*, 9, *a*) ($\lambda_1 = +4.86$, $\lambda_2 = -5.80$), meaning yield rises in one direction but falls in the other. The strong interaction term (x_1x_2 coefficient $= -5.33$, the largest in the model) controls the response: yield reached 99.7% at long reaction time with low catalyst loading (120 min, 3 wt%) but dropped to only 80.8% at long time with high loading (120 min, 5 wt%). Excess shell CaO may slow the reaction through increased viscosity of the reaction mixture, formation of calcium diglyceride on the catalyst surface, or mass transfer limitations caused by excessive solid loading in the ultrasonic field.

The mixed catalyst produced an inverted surface (Table 6, Fig. 8, *c*, 9, *c*) (both eigenvalues positive: $\lambda_1 = +7.48$, $\lambda_2 = +6.32$), confirming a minimum at the center of the design space (95.5 min, 4.18 wt%, predicted 89.6%). Yield climbed toward the corners and axial points, reaching up to 99.8%. This unusual pattern suggests that the complementary interaction between CaO and MgO is more effective under conditions that deviate from the center point. The lower R^2 for this model (0.9598 versus >0.999 for the other two) also indicates that additional factors not captured by the two-variable design may influence the mixed catalyst's performance, and a broader design could clarify this.

Effective acoustic power of 56.0 W at 28 kHz (determined by calorimetric calibration via eq. (1)) (56% of nominal 100 W) shows why calorimetric calibration matters. All catalysts produced mean yields above 89% under these conditions.

This study has several limitations. The results apply only to the small batch size used (4.8 g castor oil), and scaling behavior is unknown. The yield was determined gravimetrically, which may overestimate the true FAME conversion due to trace impurities not fully removed by washing. The reaction temperature was not controlled and rose from approximately 28 to 50°C through cavitation heating. These conditions define the boundaries within which the results are valid.

The study also has specific disadvantages. Biodiesel fuel properties (density, viscosity, flash point, cetane number) were not measured against ASTM D6751 or EN 14214, so the product quality remains unverified. Catalyst reusability was not tested, leaving the practical lifetime and regeneration requirements unknown. The two-factor CCD captured only reaction time and catalyst loading; other variables such as methanol-to-oil ratio, temperature, and catalyst particle size were held constant and their effects were not explored.

Future work should address these gaps. GC-MS analysis would provide accurate FAME purity to replace the gravimetric proxy. Testing at larger batch scales (100–500 g oil) would confirm whether the response surface patterns observed here hold under more realistic production conditions. Reusability trials over multiple reaction cycles would establish the practical economic advantage of these natural catalysts. A broader experimental design that includes temperature and methanol ratio as additional factors could clarify the unusual inverted response surface of the mixed catalyst.

7. Conclusions

1. Characterization by XRD, SEM-EDX, and FTIR confirmed that calcination at 900°C for 5 h converts shell into single-phase CaO (Ca 43.43 wt%) and limestone into mixed CaO-MgO (Ca 27.65 wt%, Mg 13.59 wt%), with distinct morphologies that reflect the dolomitic versus aragonite origin of each precursor.

2. Under calibrated ultrasonic irradiation (56.0 ± 4.2 W at 28 kHz), the mixed catalyst gave the highest mean yield (95.4 ± 4.3%), followed by limestone (93.2%) and shell (89.2%; ANOVA $F = 8.18$, $p < 0.05$). The limestone yield of 93.2% by direct calcination and sonication alone far exceeded the 16.45% reported for the same limestone without sonication, confirming that acoustic cavitation compensates for low catalyst surface area.

3. The biodiesel yield for each catalyst was described by a second-order polynomial relating two input variables (reaction time and catalyst loading) to one output variable (yield). For limestone, both linear terms were positive and both quadratic terms were negative, producing a convex surface with a maximum (97.9% at 93.9 min, 4.24 wt%); reaction time and catalyst loading had comparable influence. For shell, the interaction term dominated, producing a saddle point where increasing catalyst loading reversed the effect of longer reaction time. For the mixed catalyst, both quadratic terms were positive, producing a concave surface with a minimum at the center and yields increasing toward the design boundaries. These are three qualitatively different optimization landscapes from the same experimental design, indicating that catalyst source governs response surface geometry, not only yield magnitude.

Conflict of interest

The authors declare that they have no conflict of interest in relation to this study, whether financial, personal, authorship or otherwise, that could affect the study and its results presented in this paper.

Financing

The study was performed without financial support.

Data availability

Data will be made available on reasonable request.

Use of artificial intelligence

The following artificial intelligence tool was used during the preparation of this manuscript:

Model: ChatGPT (GPT-5.4).

Where used: overall manuscript text.

Specific task performed by AI: grammar, spelling, and punctuation checking of the English-language manuscript text.

How the authors checked AI outputs: all suggestions were reviewed line by line by the first author (A. Faizal) and the corresponding author (S. Wahyudi). No AI-generated text was adopted without human review.

Influence on conclusions: the AI tool did not influence the scientific conclusions of this study. All experimental data, analysis, interpretation, and formulation of conclusions are entirely the work of the authors.

Acknowledgments

The authors acknowledge the Laboratorium Mineral dan Material Maju, FMIPA, Universitas Negeri Malang for XRD, SEM-EDX, and FTIR characterization.

Authors' contributions

Abdullah Faizal: Conceptualization, Methodology, Investigation, Formal analysis, Data curation, Visualization, Writing – original draft; **Slamet Wahyudi**: Supervision, Project administration, Writing – review & editing; **Winarto**: Supervision, Resources; **Ishardita Pambudi Tama**: Supervision, Validation.

References

1. Farouk, S. M., Tayeb, A. M., Abdel-Hamid, S. M. S., Osman, R. M. (2024). Recent advances in transesterification for sustainable biodiesel production, challenges, and prospects: a comprehensive review. Environmental Science and Pollution Research, 31 (9), 12722–12747. https://doi.org/10.1007/s11356-024-32027-4
2. Atabani, A. E., Silitonga, A. S., Badruddin, I. A., Mahlia, T. M. I., Masjuki, H. H., Mekhilef, S. (2012). A comprehensive review on biodiesel as an alternative energy resource and its characteristics. Renewable and Sustainable Energy Reviews, 16 (4), 2070–2093. https://doi.org/10.1016/j.rser.2012.01.003
3. Banković-Ilić, I. B., Stamenković, O. S., Veljković, V. B. (2012). Biodiesel production from non-edible plant oils. Renewable and Sustainable Energy Reviews, 16 (6), 3621–3647. https://doi.org/10.1016/j.rser.2012.03.002
4. Osorio-González, C. S., Gómez-Falcon, N., Sandoval-Salas, F., Saini, R., Brar, S. K., Ramírez, A. A. (2020). Production of Biodiesel from Castor Oil: A Review. Energies, 13 (10), 2467. https://doi.org/10.3390/en13102467
5. Chidambaranathan, B., Gopinath, S., Aravindraj, R., Devaraj, A., Gokula Krishnan, S., Jeevaananthan, J. K. S. (2020). The production of biodiesel from castor oil as a potential feedstock and its usage in compression ignition Engine: A comprehensive review. Materials Today: Proceedings, 33, 84–92. https://doi.org/10.1016/j.matpr.2020.03.205
6. Lee, H. V., Juan, J. C., Taufiq-Yap, Y. H., Kong, P. S., Rahman, N. A. (2015). Advancement in heterogeneous base catalyzed technology: An efficient production of biodiesel fuels. Journal of Renewable and Sustainable Energy, 7 (3). https://doi.org/10.1063/1.4919082
7. Ponnappan, V. S., Munuswamy, D. b., Nagappan, B., Devarajan, Y. (2021). Investigation on the effect of ultrasound irradiation on biodiesel properties and transesterification parameters. Environmental Science and Pollution Research, 28 (45), 64769–64777. https://doi.org/10.1007/s11356-021-15568-w
8. Yan, S., DiMaggio, C., Mohan, S., Kim, M., Salley, S. O., Ng, K. Y. S. (2010). Advancements in Heterogeneous Catalysis for Biodiesel Synthesis. Topics in Catalysis, 53 (11-12), 721–736. https://doi.org/10.1007/s11244-010-9460-5
9. Tahvildari, K., Anaraki, Y. N., Fazaeli, R., Mirpanji, S., Delrish, E. (2015). The study of CaO and MgO heterogenic nano-catalyst coupling on transesterification reaction efficacy in the production of biodiesel from recycled cooking oil. Journal of Environmental Health Science and Engineering, 13 (1). https://doi.org/10.1186/s40201-015-0226-7
10. Ismail, S., Ahmed, A. S., Anr, R., Hamdan, S. (2016). Biodiesel Production from Castor Oil by Using Calcium Oxide Derived from Mud Clam Shell. Journal of Renewable Energy, 2016, 1–8. https://doi.org/10.1155/2016/5274917
11. Aqliliriana, C. M., Ernee, N. M., Irmawati, R. (2015). Preparation and characterization of modified calcium oxide from natural sources and their application in the transesterification of palm oil. International Journal of Scientific and Technology Research, 4 (11), 168–175.
12. Widiarti, N., Bahruji, H., Holilah, H., Ni'mah, Y. L., Ediati, R., Santoso, E. et al. (2021). Upgrading catalytic activity of NiO/CaO/MgO from natural limestone as catalysts for transesterification of coconut oil to biodiesel. Biomass Conversion and Biorefinery, 13 (4), 3001–3015. https://doi.org/10.1007/s13399-021-01373-5
13. Encinar, J. M., González, J. F., Pardal, A. (2012). Transesterification of castor oil under ultrasonic irradiation conditions. Preliminary results. Fuel Processing Technology, 103, 9–15. https://doi.org/10.1016/j.fuproc.2011.12.033

14. Abukhadra, M. R., Mohamed, A. S., El-Sherbeeny, A. M., Soliman, A. T. A., Abd Elgawad, A. E. E. (2020). Sonication induced transesterification of castor oil into biodiesel in the presence of MgO/CaO nanorods as a novel basic catalyst: Characterization and optimization. Chemical Engineering and Processing - Process Intensification, 154, 108024. https://doi.org/10.1016/j.cep.2020.108024
15. Gandhi, S. S., Gogate, P. R. (2021). Intensified transesterification of castor oil using ultrasonic horn: response surface methodology (RSM) based optimization. International Journal of Green Energy, 18 (14), 1523–1535. https://doi.org/10.1080/15435075.2021.1911808
16. Sabzimaleki, M., Ghobadian, B., Mazloom Farsibaf, M., Najafi, G., Dehghani Soufi, M., Mohammad Safieddin Ardebili, S. (2015). Optimization of Biodiesel Ultrasound-Assisted Synthesis from Castor Oil Using Response Surface Methodology (RSM). Chemical Product and Process Modeling, 10 (2), 123–133. https://doi.org/10.1515/cppm-2014-0013
17. Buasri, A., Chaiyut, N., Loryuenyong, V., Worawanitchaphong, P., Trongyong, S. (2013). Calcium Oxide Derived from Waste Shells of Mussel, Cockle, and Scallop as the Heterogeneous Catalyst for Biodiesel Production. The Scientific World Journal, 2013 (1). https://doi.org/10.1155/2013/460923